Equation of State for Turbulence in the Gross-Pitaevskii Model

Gevorg Martirosyan,[1,*] Kazuya Fujimoto,[2] and Nir Navon[3,4]

[1]*Cavendish Laboratory, University of Cambridge, J. J. Thomson Avenue, Cambridge CB3 0HE, United Kingdom*
[2]*Department of Physics, Institute of Science Tokyo, 2-12-1 Ookayama, Meguro-ku, Tokyo 152-8551, Japan*
[3]*Department of Physics, Yale University, New Haven, Connecticut 06520, USA*
[4]*Yale Quantum Institute, Yale University, New Haven, Connecticut 06520, USA*

(Received 2 August 2024; revised 19 October 2025; accepted 27 February 2026; published 14 April 2026)

We report the numerical observation of a far-from-equilibrium equation of state (EOS) in the Gross-Pitaevskii (GP) model. We first show that the momentum distribution of the turbulent cascade is well described by wave-turbulent kinetic theory in the appropriate limits. Calculating the energy and particle fluxes $\Pi_\epsilon(k)$ and $\Pi_N(k)$, we show that the turbulent state possesses the hallmarks of a direct energy cascade. Building on this, we show that the GP model encodes a universal EOS in the form of a relationship between the turbulent cascade's momentum distribution amplitude n_0 and the energy flux ϵ in the steady state. We find that in our regime of "mixed" turbulence—where both vortices and waves play a significant role—$n_0 \propto \epsilon^{0.67(2)}$, a result that is not captured by any existing theory of turbulence but that agrees with a recent experimental measurement for large energy fluxes. Finally, we find that the concept of quasi-static thermodynamic processes between equilibrium states extends to far-from-equilibrium steady states.

DOI: 10.1103/1ppc-pl4k

Introduction—Equilibrium and near-equilibrium thermodynamics form conceptual cornerstones of physics, reducing the behavior of complex many-body systems to relations among a few macroscopic observables. Far from equilibrium, such a unifying framework is lacking, and unveiling universal features has become a major goal of modern physics. When local equilibrium holds, local thermodynamics and hydrodynamics provide a bridge to universal descriptions [1–3]. Even without microscopic equilibrium, universal phenomena have been predicted and observed—ranging from thermalization of far-from-equilibrium states [4–11] to steady states characterized by state variables linked through far-from-equilibrium analogs of equations of state (EOS) [12–14].

A remarkable example of steady states that remain locally far from equilibrium is matter-wave turbulence, sustained by energy injection and dissipation at distinct length scales. Such cascades have recently been realized in ultracold-atom systems [15–17], where a far-from-equilibrium EOS was measured [14]. All tractable theoretical descriptions of these experiments rely on the classical-field Gross-Pitaevskii (GP) equation [18–22].

*Contact author: gevorgmartirosyan97@gmail.com

Although the GP model has been studied for decades [25,26], and its equilibrium and near-equilibrium behavior are well established, much of its far-from-equilibrium physics remains to be understood. It supports regimes such as Kolmogorov vortex turbulence [17,27–31] and weak-wave turbulence (WWT) [32,33], which feature a far-from-equilibrium EOS relating the amplitude of a steady-state spectrum to an energy flux. However, these solutions do not describe the recently measured experimental EOS [14], motivating a calculation of the EOS within the GP model in the same setting as the experiments.

In this Letter, we perform simulations of the GP model in the setting of the experiments [14] and show that the GP model possesses a far-from-equilibrium EOS that lies outside any known paradigm of turbulence. The turbulent state obtained at long times is steady and we find that it is characterized by a momentum distribution quantitatively described by a universal prediction from WWT theory. This steady state possesses the hallmarks of a direct energy cascade, i.e., that the dissipation-scale-independent energy flux is scale invariant, transporting energy from large to small length scales. However, the power-law scaling of the amplitude of the momentum distribution with the energy flux is starkly different from predictions of any theory of turbulence, but agrees well with the experimental EOS for large values of the energy flux.

The model—Our study is based on the universal GP model

$$i\hbar\frac{\partial\psi}{\partial t} = \left(-\frac{\hbar^2}{2m}\nabla^2 + g|\psi|^2\right)\psi, \tag{1}$$

for the field $\psi(\boldsymbol{r}, t)$. This equation, also known as the nonlinear Schrödinger equation, is a universal wave equation that describes a variety of systems, such as optical fields in nonlinear Kerr media [34], weakly interacting Bose-Einstein condensates [35], and gravity waves in deep inviscid fluids [36]. We focus on the system of the weakly interacting Bose gas in 3D, where $\psi(\boldsymbol{r}, t)$ is interpreted as the classical field of the Bose gas, $g = 4\pi\hbar^2 a/m$ is the strength of the interatomic interactions, m is the atomic mass, and a is the s-wave scattering length [37]. The field is normalized to $\int |\psi(\boldsymbol{r}, t)|^2 \mathrm{d}^3\boldsymbol{r} = N$, where N is the (instantaneous) particle number.

To study universal steady-state properties of the GP model far from equilibrium, one has to supplement forcing and dissipation mechanisms into Eq. (1); here we do that by adding a potential term of the form $V(\boldsymbol{r}, t) = V_{\mathrm{drive}}(\boldsymbol{r}, t) + V_{\mathrm{diss}}(\boldsymbol{r}) + V_{\mathrm{box}}(\boldsymbol{r})$ (see Supplemental Material [38]). The first term is a forcing at the length scale of the system size L, $V_{\mathrm{drive}}(\boldsymbol{r}, t) = U_{\mathrm{s}} \sin(\omega t) z/L$. The second term implements small-length-scale dissipation. This dissipation term is critical for realizing a steady state in a continuously forced system; we choose V_{diss} to mimic the dissipation encountered in experiments, *i.e.*, evaporative losses when the atom energy exceeds an energy U_{D} [16]. The last term, V_{box}, is a confining potential; for experimental relevance we pick a cylindrical box potential [14,42] whose axis is oriented along the shaking direction z [see the cartoon of Fig. 1(a)] [43]. Recent experimental studies have confirmed that this classical field approach is useful for describing a wave-turbulent scale-invariant steady state of a quantum degenerate Bose gas [15,16].

The system is initialized in the ground state of Eq. (1) including $V_{\mathrm{box}}(\boldsymbol{r})$, which corresponds to a Bose-Einstein condensate with a nearly uniform density, except near the boundary of the box. For relevance, we use numbers typical of recent experiments [14]: a box radius $R = 15$ μm and length $L = 50$ μm, an initial atom number $N(t = 0) = 2 \times 10^5$, and a/a_0 between 25 and 400 (where a_0 is the Bohr radius). The natural energy scale of the system $\zeta \equiv gn(t = 0)$ therefore varies between $k_{\mathrm{B}} \times 1.2$ nK and $k_{\mathrm{B}} \times 19$ nK, the corresponding timescale $\tau \equiv h/\zeta$, between 2.6 ms and 42 ms, and the natural length scale $\xi \equiv \hbar/\sqrt{2m\zeta}$, between 0.6 μm and 2.3 μm (using the mass m of ^{39}K); $n = N/V$ is the average density, where $V = \pi R^2 L$ is the box volume. The gas is driven at a frequency $\omega/(2\pi)$ that matches the resonance of the lowest-lying Bogoliubov excitation [44]; for our set of parameters, $\omega/(2\pi)$ ranges from 5 to 20 Hz.

Momentum distribution—As shown in Fig. 1(b), the injection of energy results in a cascade front propagating to higher momenta, until hitting the momentum k_{D} [45] at a time $t \approx t_{\mathrm{D}}$ [46]. For $t \gtrsim t_{\mathrm{D}}$, the system is in a steady state well described by a power law distribution for the mode occupation number: $N_k \propto k^{-\gamma}$ with $\gamma \approx 3.5$. Here, N_k is the mode occupation number for the states of momentum k, normalized as $\sum_{\boldsymbol{k}} N_k = N$; in the continuous limit, it is related to the momentum distribution $n(k)$ as $N_k = ((2\pi)^3/V) n(k)$.

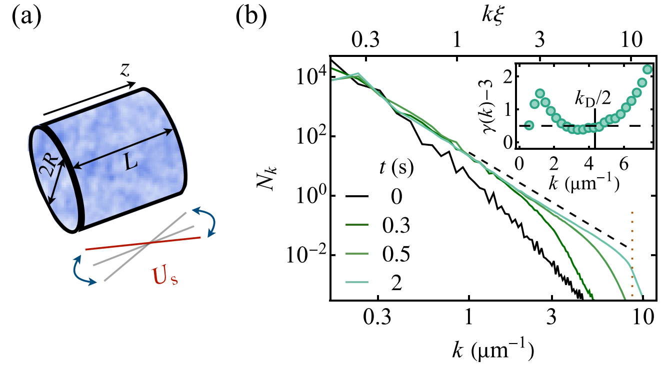

FIG. 1. The direct turbulent cascade in the GP model. (a) Cartoon of the simulation geometry and the driving protocol. We use a cylindrical box trapping potential of length L and radius R, and the energy is injected into the system by applying a time-periodic potential gradient $V_{\mathrm{drive}}(\boldsymbol{r}, t) = U_{\mathrm{s}} \sin(\omega t) z/L$ (see text for typical parameters). (b) The build-up of the turbulent cascade; the mode occupation number N_k is shown for various shaking times t. At long times, the system is in a steady state with $N_k \propto k^{-\gamma}$ (the dashed line corresponds to $\gamma = 3.5$). The inset shows the cascade exponent $\gamma(k) \equiv -\mathrm{d}\ln[n(k)]/\mathrm{d}\ln[k]$, calculated from the continuous momentum distribution $n(k)$; the dashed line is $\gamma(k) = 3.5$. Here, the simulation parameters are $L = 50$ μm, $R = 15$ μm, $U_{\mathrm{s}} = 1.0\zeta$, $\omega = 2\pi \times 10$ Hz, and $a = 100a_0$ (corresponding to $\xi = 1.2$ μm and $\tau = 10$ ms).

We systematically studied the momentum-resolved cascade exponent $\gamma(k) \equiv -\mathrm{d}\ln[n(k)]/\mathrm{d}\ln[k]$ across interaction strengths (different ξ) and find that $\gamma(k\xi)$ is in excellent agreement with the 4-wave WWT prediction $3 + 1/(3\ln[k/k_{\mathrm{F}}])$, provided that k_{F} is replaced by $k_0 = 1.64(2)k_\xi$ (see End Matter and Fig. 5). In other words, the isotropic 4-wave cascade's effective injection scale is set by the GPE scale $1/\xi$ instead of the physical injection scale k_{F}. However, as was already presumed experimentally [14,15], we find that a power law $n(k) \propto k^{-\gamma_0}$ with an effective exponent $\gamma_0 = 3.5$ accurately captures all the relevant details, since the variation of the logarithmic correction for $\gamma(k)$ is small over the relevant momentum range [47] (see also a discussion in Ref. [38]). From now on, we fix $n(k)$ to this power law and define the amplitude of the power law $n_0 \equiv N_k k^3 (k\xi)^{\gamma_0 - 3}$.

Energetics of the turbulent cascade—We next turn to the calculation of the energy-density input and dissipation rates. As energy is injected into the system only by the forcing V_{drive}, the energy input rate can be calculated as $\epsilon_{\mathrm{in}} \equiv \langle Fvn \rangle$, where $F \equiv -\hat{z} \cdot \nabla V_{\mathrm{drive}}$, $\hat{z}$ is the unit vector along z, v is the center-of-mass velocity of the gas and the averaging $\langle\cdot\rangle$ is performed over a drive period. The energy is dissipated at high momenta solely by particles with momenta $k > k_{\mathrm{D}}$ leaving the trap. Hence, in previous experimental works [14,16], the energy dissipation rate was reasonably assumed to be $\dot{N} U_{\mathrm{D}}$ where $\dot{N}$ is the particle loss rate. However, as shown in Fig. 2(a) for three different U_{s}, the energy-density injection rate ϵ_{in} is consistently

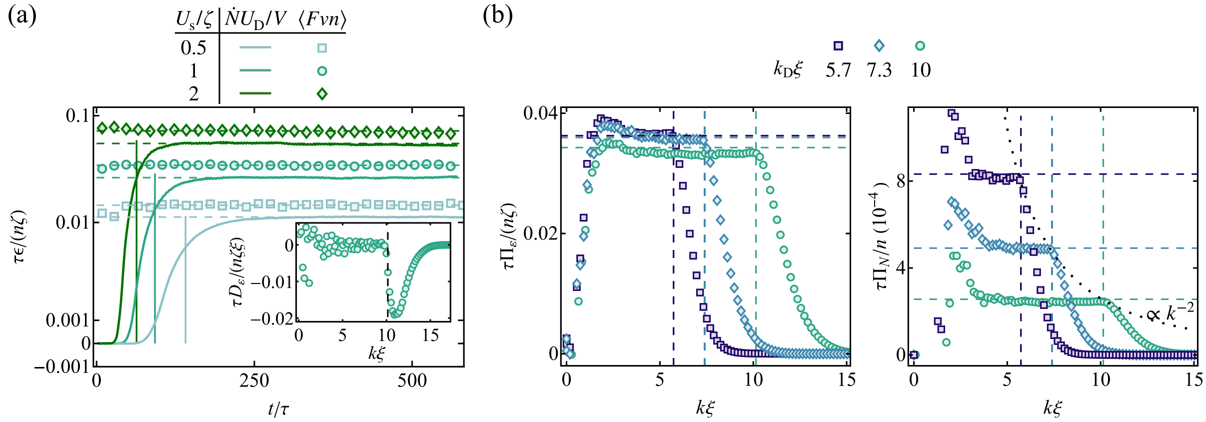

FIG. 2. Energetics of the direct turbulent cascade. (a) Energy input and dissipation rates. We show $\tau\epsilon/(n\zeta)$, where ϵ is either the energy injection rate calculated as $\epsilon_{\text{in}} \equiv \langle Fvn\rangle$ (symbols) or the particle dissipation rate $\dot{N}$ multiplied by U_D/V (solid lines). Both ϵ_{in}/n and $\dot{N}U_D/N$ are constant at long times (dashed lines; see also Supplemental Material [38]), but ϵ_{in}/n is higher by a factor of ≈ 1.3. The vertical solid lines mark the onset time of dissipation t_D; for an analytical calculation of t_D, see the End Matter. Inset: the dissipation spectrum D_ε for $U_s = \zeta$ and $a = 100a_0$. The average dissipation momentum $\langle k_{\text{diss}}\rangle \approx 1.15k_D$, predicting $\epsilon V/(\dot{N}U_D) \approx 1.32$ (see text). (b) Energy flux Π_ε (left) and particle flux Π_N (right) for different dissipation scales k_D (vertical dashed lines). Both fluxes are scale independent. The dotted line ($\propto k^{-2}$) shows that $\Pi_N \propto k_D^{-2}$, while Π_ε is (nearly) independent of k_D; horizontal dashed lines are ϵ_{in} (resp. $\tau\dot{N}/N$) in the left (resp. right) panel (see text).

higher than $\dot{N}U_D/V$. The reason for $\epsilon_{\text{in}} > \dot{N}U_D/V$ stems from the shape of the dissipation spectrum $D_\varepsilon(k)$ (see Supplemental Material [38] for a formal definition): calculating the energy-density dissipation rate as $\dot{N}U_D/V$ assumes that the dissipation happens exactly at energy U_D. As shown in the inset of Fig. 2(a) for $U_s = \zeta$, $D_\varepsilon(k)$ has a sharp onset at k_D, but has a significant tail above k_D. The average dissipation momentum is $\langle k_{\text{diss}}\rangle \equiv \int kD_\varepsilon(k)\mathrm{d}k/\int D_\varepsilon(k)\mathrm{d}k \approx 1.15k_D$ [48], showing that the energy dissipated from the system per unit time is $\approx 1.32\dot{N}U_D$. This is in excellent agreement with $\alpha \equiv V\epsilon_{\text{in}}/(\dot{N}U_D)$ [49] [see the End Matter for a systematic study of α versus interaction strength and U_s, showing that $\alpha \approx 1.3$].

Having verified that the energy input rate (at low k) and dissipation rate (at high k) are equal, we turn to the direct calculation of the scale-resolved energy flux $\Pi_\varepsilon(k)$ and particle flux $\Pi_N(k)$ (see Supplemental Material [38] for the formal definition of the fluxes). As shown in Fig. 2(b) in the steady state, Π_ε is momentum independent in the *inertial range*, a certain range of momenta where neither forcing nor dissipation takes place; this flux transports the energy injected at low k to higher k, up to k_D. Importantly, Π_ε in the inertial range is equal to ϵ_{in}. As expected for an energy cascade, Π_ε is also (nearly) independent of the dissipation scale k_D [50]. On the other hand, Π_N is also momentum independent in steady state, but its plateau value decreases as $\propto k_D^{-2}$, as expected for particles with a quadratic dispersion relation [see dotted line in the right panel of Fig. 2(b)] [51]. We define ϵ, the scale-invariant energy-density flux, as the plateau value of Π_ε; in the rest of the Letter we compute ϵ as $\langle Fvn\rangle$.

EOS for turbulence—Finally, we investigate the relation between the two far-from-equilibrium state variables of the system, ϵ and n_0. Figure 3(a) shows n_0 and ϵ for different a; we express both state variables using the instantaneous natural scales of the GP equation ξ_t, τ_t, and ζ_t defined through the instantaneous density n [53]. Data for different values of a fall on a (nearly) universal curve, demonstrating that the only relevant scales describing the turbulent cascade are the intrinsic scales of the universal GP model Eq. (1) and all the dependence on the system and drive scales (L, R, U_s, ω, k_D) drops out [54].

The data of Fig. 3(a) show that the GP model contains a turbulent EOS that is a power law of the form $n_0/n = C(\tau_t\epsilon/[n\zeta_t])^b$, with $C = 29(2)$ and $b = 0.67(2)$, which is not described by known paradigms of turbulence. The two broad paradigms are wave (compressible-energy dominated) and vortex (incompressible-energy dominated) turbulence. Our b is inconsistent with any wave-kinetic description, as a kinetic theory with ℓ-wave interactions predicts an exponent $b = 1/(\ell - 1) \leq 0.5$. Furthermore, the most plausible 4-wave theory predicts that the relation between n_0 and ϵ would have to be independent of the total density n, which is not the case for the EOS constructed here [55,56].

To go further, we decompose in [38] the energy spectrum into compressible and incompressible parts [27] and show that while the compressible part is typically larger than the incompressible one in the k range used to extract n_0, the two are of the same magnitude; moreover, the incompressible part increases more rapidly with ϵ (similar observations were also recently reported in [21]). The observed EOS is therefore likely a result of an interplay between compressible (wave) and incompressible (vortex) excitations. As far as we

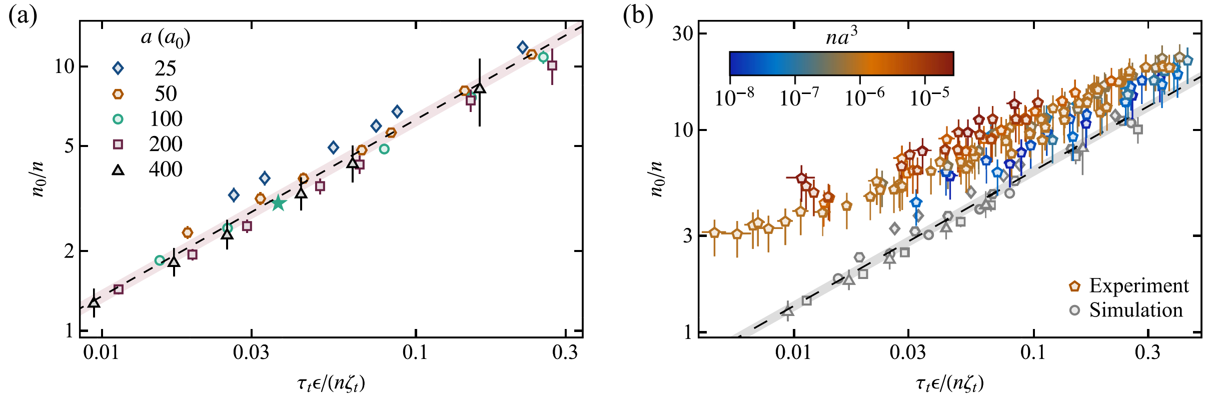

FIG. 3. A universal equation of state of the GP model. (a) The numerical calculations for different a collapse onto a universal curve when the state variables ϵ and n_0 are expressed in the instantaneous natural scales of the GP model (n, ξ_t, ζ_t, τ_t). The dashed line is a power-law fit to the data that gives $n_0/n = 29(2)(\tau_t\epsilon/[n\zeta_t])^{0.67(2)}$, and the pink band shows the fit uncertainty. (b) The comparison of our numerical EOS (gray symbols) with the experimental data from [14] (colored symbols). The color coding of the experimental data is based on the gas parameter na^3; note that the experimental fluxes are multiplied by 1.3 compared to the data of [14] to account for $\alpha \neq 1$. The vertical error bars of the experimental data represent the uncertainties due to different γ_0 in simulations and experiments (see Supplemental Material [38]).

are aware, there is no existing theory that describes this regime of "mixed" quantum turbulence and the shape of the EOS remains to be understood. We further note that the value of b being the same as the exponent of the scaling of the energy spectrum for vortex (i.e., hydrodynamic) turbulence $E_{\mathrm{K41}} \propto \epsilon^{2/3}$ [57] is likely coincidental, as this prediction is for the incompressible energy spectrum while our EOS is for the momentum distribution; besides, our computed incompressible energy spectra are also distinct from the K41 prediction [38]. We note, however, that Kolmogorov turbulence can also be realized and measured in ultracold-atom experiments [17] (for $k\xi \ll 1$) but in that case the K41 spectrum originates from (coarse-grained) velocity field rather than the (atomic) momentum distribution.

In Fig. 3(b) we compare our calculations (grey symbols) with the experimental measurements [14] (colored symbols); see also Supplemental Material [38] for details. The experimental data are above the numerical results. Note that the experimental data do not represent a universal EOS on this plot: they collapse onto a single curve when both axes are rescaled with empirically determined powers of the gas parameter na^3 [14], a scaling that is inherently beyond the GP model. However, we note that in the limit $n \to \infty$ and $na^3 \to 0$ the GP model is expected to be a good description of the experimental setting, and Fig. 3(b) shows that the experimental data appear to approach our numerical results for lower na^3.

Finally, we note that the slow decrease of N due to evaporative losses above k_{D} implements a slow thermodynamic-like process. Indeed, as N decreases, the state variable $\epsilon \propto N$ also decreases, resulting in a slow change of the far-from-equilibrium state (see also Supplemental Material [38]). In Fig. 4, we show that the simultaneous change of the state variables ϵ and n_0 follows the EOS: when rescaled to the instantaneous GP scales, the instantaneous ϵ and n_0 "slide up" on our universal EOS line over time, see blue to red shades [58]. This is reminiscent of the concept of thermodynamic quasi-static processes, for which infinitesimal changes of external constraints take a system through a dense succession of equilibrium states [59]. Remarkably, we find that this concept generalizes to states that are even locally far from equilibrium.

Conclusions—We numerically investigated the properties of a turbulent cascade arising in the GP model when a box-trapped gas is periodically driven, and showed that it can be described by a universal EOS relating the turbulent state variables, the energy flux and the cascade amplitude. The form of our EOS is inconsistent with any existing

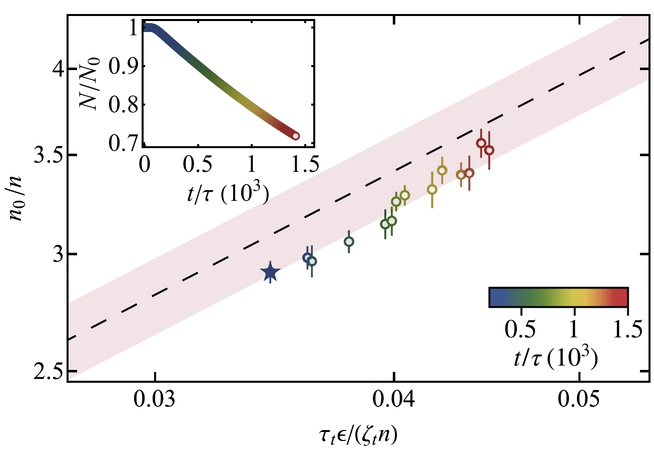

FIG. 4. Quasistatic process far from equilibrium. The instantaneous far-from-equilibrium state variables for different t follow the EOS, in analogy with a quasi-static process in equilibrium thermodynamics. The data correspond to $a = 100a_0$ and the blue star here corresponds to the green star in Fig. 3(a). The inset shows the fraction of particles N/N_0 left in the system.

theory of turbulence, posing a new theoretical challenge. Furthermore, the comparison of our classical-field simulations to experimental measurements provides valuable benchmarks for testing the validity of classical-field theories in far-from-equilibrium scenarios. Namely, we find that the GP model provides valuable insight into the experimental results of [14], even if it fails to fully capture the equation of state—indeed, the observed na^3 scaling is incompatible with the universal GP framework (see also Supplemental Material [38]). This partial success is nevertheless striking given that there is no firm theoretical justification for its applicability in this turbulent regime. Understanding the foundations of this success, and developing refined approaches that incorporate quantum effects, remain important challenges for the field. One should also investigate the fluctuations of N_k; comparing these fluctuations between experiments and classical field simulations could shed light on the role of quantum fluctuations in turbulent quantum fluids.

Acknowledgments—We thank M. Gazo, J. Etrych, C. Eigen, G. Krstulovic, M. Tsubota, G. Falkovich, and V. L'vov for discussions. This work was supported by the NSF (Grants No. PHY-1945324 and No. PHY-2110303), DARPA (Grant No. HR00112320038), the David and Lucile Packard Foundation, the Alfred P. Sloan Foundation, and JSPS KAKENHI (Grant No. JP23K13029). G. M. acknowledges support from Trinity College (Cambridge) and Yale University for its hospitality.

[1] P. C. Hohenberg and B. I. Halperin, Theory of dynamic critical phenomena, Rev. Mod. Phys. **49**, 435 (1977).
[2] A. J. Bray, Theory of phase-ordering kinetics, Adv. Phys. **51**, 481 (2002).
[3] D. Forster, *Hydrodynamic Fluctuations, Broken Symmetry, and Correlation Functions* (CRC Press, Reading, Massachusetts, 2018).
[4] J. Berges, A. Rothkopf, and J. Schmidt, Nonthermal fixed points: Effective weak coupling for strongly correlated systems far from equilibrium, Phys. Rev. Lett. **101**, 041603 (2008).
[5] S. Erne, R. Bücker, T. Gasenzer, J. Berges, and J. Schmiedmayer, Universal dynamics in an isolated one-dimensional Bose gas far from equilibrium, Nature (London) **563**, 225 (2018).
[6] M. Prüfer, P. Kunkel, H. Strobel, S. Lannig, D. Linnemann, C.-M. Schmied, J. Berges, T. Gasenzer, and M. K. Oberthaler, Observation of universal dynamics in a spinor Bose gas far from equilibrium, Nature (London) **563**, 217 (2018).
[7] J. A. P. Glidden, C. Eigen, L. H. Dogra, T. A. Hilker, R. P. Smith, and Z. Hadzibabic, Bidirectional dynamic scaling in an isolated Bose gas far from equilibrium, Nat. Phys. **17**, 457 (2021).
[8] S. Huh, K. Mukherjee, K. Kwon, J. Seo, J. Hur, S. I. Mistakidis, H. R. Sadeghpour, and J.-y. Choi, Universality class of a spinor Bose-Einstein condensate far from equilibrium, Nat. Phys. **20**, 402 (2024).
[9] M. Moreno-Armijos, A. R. Fritsch, A. García-Orozco, S. Sab, G. Telles, Y. Zhu, L. Madeira, S. Nazarenko, V. I. Yukalov, and V. S. Bagnato, Observation of relaxation stages in a non-equilibrium closed quantum system: Decaying turbulence in a trapped superfluid, Phys. Rev. Lett. **134**, 023401 (2025).
[10] M. Gazo, A. Karailiev, T. Satoor, C. Eigen, M. Gałka, and Z. Hadzibabic, Universal coarsening in a homogeneous two-dimensional Bose gas, Science **389**, 802 (2025).
[11] G. Martirosyan, M. Gazo, J. Etrych, S. M. Fischer, S. J. Morris, C. J. Ho, C. Eigen, and Z. Hadzibabic, A universal speed limit for spreading of coherence, Nature (London) **647**, 608 (2025).
[12] S. C. Takatori and J. F. Brady, Towards a thermodynamics of active matter, Phys. Rev. E **91**, 032117 (2015).
[13] F. Ginot, I. Theurkauff, D. Levis, C. Ybert, L. Bocquet, L. Berthier, and C. Cottin-Bizonne, Nonequilibrium equation of state in suspensions of active colloids, Phys. Rev. X **5**, 011004 (2015).
[14] L. H. Dogra, G. Martirosyan, T. A. Hilker, J. A. P. Glidden, J. Etrych, A. Cao, C. Eigen, R. P. Smith, and Z. Hadzibabic, Universal equation of state for wave turbulence in a quantum gas, Nature (London) **620**, 521 (2023).
[15] N. Navon, A. L. Gaunt, R. P. Smith, and Z. Hadzibabic, Emergence of a turbulent cascade in a quantum gas, Nature (London) **539**, 72 (2016).
[16] N. Navon, C. Eigen, J. Zhang, R. Lopes, A. L. Gaunt, K. Fujimoto, M. Tsubota, R. P. Smith, and Z. Hadzibabic, Synthetic dissipation and cascade fluxes in a turbulent quantum gas, Science **366**, 382 (2019).
[17] M. Zhao, J. Tao, and I. B. Spielman, Kolmogorov scaling in turbulent 2D Bose-Einstein condensates, Phys. Rev. Lett. **134**, 083402 (2025).
[18] I. Chantesana, A. Piñeiro Orioli, and T. Gasenzer, Kinetic theory of nonthermal fixed points in a Bose gas, Phys. Rev. A **99**, 043620 (2019).
[19] Y. Sano, N. Navon, and M. Tsubota, Emergent isotropy of a wave-turbulent cascade in the Gross-Pitaevskii model, Europhys. Lett. **140**, 66002 (2022).
[20] Y. Zhu, B. Semisalov, G. Krstulovic, and S. Nazarenko, Direct and inverse cascades in turbulent Bose-Einstein condensates, Phys. Rev. Lett. **130**, 133001 (2023).
[21] T. Z. Fischer and A. S. Bradley, Regimes of steady-state turbulence in a quantum fluid, Phys. Rev. A **111**, 023308 (2025).
[22] This model is not limited to weakly interacting BECs; it also applies in the classical-field limit of highly occupied modes [23,24].
[23] A. Sinatra, C. Lobo, and Y. Castin, Classical-field method for time dependent Bose-Einstein condensed gases, Phys. Rev. Lett. **87**, 210404 (2001).
[24] K. B. Davis, S. A. Morgan, and K. Burnett, Simulations of thermal Bose fields in the classical limit, Phys. Rev. A **66**, 053618 (2002).
[25] G. Fibich, *The Nonlinear Schrödinger Equation* (Springer, New York, 2015), Vol. 192.
[26] L. Pitaevskii and S. Stringari, *Bose–Einstein Condensation and Superfluidity* (Oxford University Press, Oxford, 2016).
[27] C. Nore, M. Abid, and M. E. Brachet, Kolmogorov turbulence in low-temperature superflows, Phys. Rev. Lett. **78**, 3896 (1997).

[28] M. Kobayashi and M. Tsubota, Kolmogorov spectrum of superfluid turbulence: Numerical analysis of the Gross–Pitaevskii equation with a small-scale dissipation, Phys. Rev. Lett. **94**, 065302 (2005).

[29] M. Tsubota, K. Fujimoto, and S. Yui, Numerical studies of quantum turbulence, J. Low Temp. Phys. **188**, 119 (2017).

[30] M. Kobayashi, P. Parnaudeau, F. Luddens, C. Lothodé, L. Danaila, M. Brachet, and I. Danaila, Quantum turbulence simulations using the Gross–Pitaevskii equation: High-performance computing and new numerical benchmarks, Comput. Phys. Commun. **258**, 107579 (2021).

[31] T. Tanogami, Theoretical analysis of quantum turbulence using the Onsager ideal turbulence theory, Phys. Rev. E **103**, 023106 (2021).

[32] V. E. Zakharov, V. S. L'vov, and G. Falkovich, *Kolmogorov Spectra of Turbulence* (Springer, Berlin, 1992).

[33] S. Nazarenko, *Wave Turbulence* (Springer, New York, 2011).

[34] G. P. Agrawal, Nonlinear fiber optics, in *Nonlinear Science at the Dawn of the 21st Century* (Springer, New York, 2000), pp. 195–211.

[35] P. G. Kevrekidis, D. J. Frantzeskakis, and R. Carretero-González, *Emergent Nonlinear Phenomena in Bose-Einstein Condensates: Theory and Experiment* (Springer, New York, 2008), Vol. 45.

[36] W. Craig, C. Sulem, and P.-L. Sulem, Nonlinear modulation of gravity waves: A rigorous approach, Nonlinearity **5**, 497 (1992).

[37] It is worthwhile noting that, as in the recent experiments [14,15], our Letter remains in a regime $ka \ll 1$, where k is the highest momentum considered. The scattering cross-section is thus momentum independent and $g = 4\pi\hbar^2 a/m$.

[38] See Supplemental Material at http://link.aps.org/supplemental/10.1103/1ppc-pl4k for the details of our simulations, calculation details for momentum-resolved fluxes, comments on the sharpness of the cascade front, the details of time dependence of state variables, comparisons of our results to experiments and weak wave turbulence theory, and an analysis of compressible and incompressible parts of the energy spectrum, which includes Refs. [39–41].

[39] G. E. Falkovich and I. V. Ryzhenkova, Kolmogorov spectra of Langmuir and optical turbulence, Phys. Fluids B **4**, 594 (1992).

[40] Note that the hydrodynamic kinetic energy is not equal to the total kinetic energy, as the latter also contains a contribution from density modulations, $\propto |\nabla\sqrt{n(\mathbf{r})}|^2$, usually referred to as quantum pressure. Though this component has been discussed before (see, *e.g.*, Refs. [27,31]), its role in neither vortex nor wave turbulence is well understood, and we do not focus on this term here.

[41] A. Cidrim, A. C. White, A. J. Allen, V. S. Bagnato, and C. F. Barenghi, Vinen turbulence via the decay of multicharged vortices in trapped atomic Bose-Einstein condensates, Phys. Rev. A **96**, 023617 (2017).

[42] N. Navon, R. P. Smith, and Z. Hadzibabic, Quantum gases in optical boxes, Nat. Phys. **17**, 1334 (2021).

[43] Note that even though the trap shape affects large-scale properties, the far-from-equilibrium state at smaller scales is largely insensitive to the details of the confining potential.

[44] S. J. Garratt, C. Eigen, J. Zhang, P. Turzák, R. Lopes, R. P. Smith, Z. Hadzibabic, and N. Navon, From single-particle excitations to sound waves in a box-trapped atomic Bose-Einstein condensate, Phys. Rev. A **99**, 021601(R) (2019).

[45] For convenience, we refer to the wavenumber $\mathbf{k}$ as momentum, even though formally the momentum is $\mathbf{p} = \hbar\mathbf{k}$.

[46] In End Matter, we derive an analytic expression for t_{D} in terms of the cascade properties.

[47] Note that [20] speculated that the steeper effective exponent could be due to the logarithmic correction. However, this Letter assumes that there is no BEC, but the presence of the BEC is crucial for understanding the effective injection scale $k_0 \propto k_\xi$, hence [20] cannot make quantitative comparisons to the experiment [15].

[48] A simple geometric picture is that particles hitting the box at non-normal incidence can remain trapped for some time even if their kinetic energy $\hbar^2k^2/(2m) > U_{\mathrm{D}}$.

[49] Even though $\alpha \neq 1$ means that the energy-density flux is not $\dot{N}U_{\mathrm{D}}/V$, the fact that α has only a very weak dependence on a ($\propto a^{0.08(1)}$) and is independent of U_{s} suggests that the determination of the energy flux via $\dot{N}U_{\mathrm{D}}/V$, as done in [14,16], will only introduce a small, presumably system-specific, systematic error.

[50] Note that the slow decrease of the plateau of Π_ϵ is due to a progressive depletion of the condensate, which results in a (slow) decrease of ϵ_{in} [corresponding horizontal dashed lines in left panel of Fig. 2(b)].

[51] Note that it is only in the limit $k_{\mathrm{D}} \to \infty$ that one recovers the expected limits $\Pi_\epsilon \to \epsilon$ with $\Pi_N \to 0$ for the direct energy cascade [52].

[52] S. Dyachenko, A. Newell, A. Pushkarev, and V. Zakharov, Optical turbulence: Weak turbulence, condensates and collapsing filaments in the nonlinear Schrödinger equation, Physica (Amsterdam) **57D**, 96 (1992).

[53] Note that ξ_t is not directly present in the axes of Fig. 3, but is used in the calculation of $n_0 = N_k k^3 (k\xi_t)^{0.5}$.

[54] The independence of our EOS with k_{D} presumably will not hold for large enough k_{D} (beyond what we studied), as it is reasonable to expect that as $k \to \infty$ (with $k < k_{\mathrm{D}}$), WWT results should be recovered.

[55] For an extensive comparison of our EOS to the prediction of 4-wave theory (as well as how the respective N_k can be deduced), see Sec. VII and Fig. S3 [38].

[56] The factor of $\xi^{0.5}$ on the y axis is a finite-k_{D} effect, but even in its absence our EOS would depend on n; within the GP model, only the WWT prediction of a power-law EOS with an exponent of $1/3$ is independent of n.

[57] U. Frisch, *Turbulence: The Legacy of A.N. Kolmogorov* (Cambridge University Press, Cambridge, England, 1995).

[58] As shown in [38], n_0 and ϵ/n are roughly constant over time, resulting in the increase of n_0/n and $\tau_t\epsilon/(n\zeta_t)$. The points in Fig. 3(a) correspond to shaking times $\approx 2t_{\mathrm{D}}$.

[59] H. B. Callen, *Thermodynamics and an Introduction to Thermostatistics* (John Wiley & Sons, New York, 1991).

[60] M. Gałka, P. Christodoulou, M. Gazo, A. Karailiev, N. Dogra, J. Schmitt, and Z. Hadzibabic, Emergence of isotropy and dynamic scaling in 2D wave turbulence in a homogeneous Bose gas, Phys. Rev. Lett. **129**, 190402 (2022).

[61] One might expect $\gamma(k)$ to be universal in the range $k_{\mathrm{F}} \ll k \ll k_{\mathrm{D}}$. We instead observe universal behavior for

$k\xi \gtrsim 2.5$, where $n(k)$ is isotropic [19,60] and $\gamma(k)$ is well defined. For $k\xi \lesssim 2.5$, our numerical resolution of $\gamma(k)$ is insufficient to make a definitive claim.

[62] At lower momenta ($k \lesssim k_\xi$) the particles interact more strongly, and the 4-wave WWT description is not expected to work. In the presence of a condensate, the proper quasiparticles to consider for $k\xi \lesssim 1$ are the Bogoliubov phonons, for which the appropriate WWT description is a wave-kinetic equation with 3-wave interactions. In our simulations, a description in terms of an equilibrium-like condensate is meaningless since for our strong drives, the Bogoliubov approximation is invalid.

[63] Interestingly, a recent experiment has observed that the momentum distribution of 2D shaken Bose gases also becomes isotropic at $k \approx k_\xi$ [60].

[64] Experimentally, k_D is bounded, so the separation between the injection scale $k_0 \propto k_\xi$ and k_D—and hence the region where the 4-wave WWT theory is applicable—is reduced for stronger interactions.

End Matter

The cascade exponent γ—In any real system, the momentum range over which universal turbulent properties (i.e., injection and dissipation independent, boundary condition independent, etc.) may exist is finite, and the observations might depend on the separation between the injection and dissipation scales. To test the universality of our steady-state $n(k)$, we calculate the apparent cascade exponent $\gamma(k) \equiv -\mathrm{d}\ln[n(k)]/\mathrm{d}\ln[k]$ for different ξ and k_D. As shown in Fig. 5, when γ is plotted versus k for various ξ (but same k_D), it decreases for $k \lesssim k_D/2$ and depends on ξ; for $k \gtrsim k_D/2$, finite-k_D effects become important and all $\gamma(k)$ increase together. However, when plotted against $k\xi$—the only dimensionless parameter for the infinite-size system—the data collapse onto a single curve in the intermediate regime $2.5 \lesssim k\xi \lesssim k_D\xi/2$ [61].

As the momentum $k_\xi \equiv 1/\xi$ marks the typical momentum scale associated with interactions, we have that for $k \gg k_\xi$, our system is weakly nonlinear and can be described by the theory of WWT [32,33]. In this weakly interacting limit (not to be confused with the criterion $na^3 \ll 1$), Eq. (1) reduces to so-called 4-wave (particle-number conserving) interactions [33], and WWT in this case predicts that the momentum distribution of the direct energy cascade has the asymptotic isotropic form $n(k) \propto k^{-3}\ln^{-1/3}(k/k_0)$ where k_0 is the energy injection scale [20,62].

The collapse in Fig. 5 shows that, despite the fact that the energy is physically injected at the scale $k_F \approx \pi/L$, the effective injection scale for the isotropic cascade is actually $k_0 \propto k_\xi$ ($\gg k_F$) [63]. To test the asymptotic form $n(k) \propto k^{-3}\ln^{-1/3}(k/k_0)$, we fit $\gamma(k)$ with $3 + 1/(3\ln[Ak\xi])$ in the regime where the numerical data overlap. We find that for $A = 0.61(1)$, the fit captures the data well. Equivalently, this fit predicts that the injection scale for the isotropic 4-wave cascade is $k_0 = 1.64(2)k_\xi$ (as long as $k_F \ll k_\xi$ [64]). The convergence towards a robust steady state, i.e., that is independent of ξ, ω, k_D, and U_s, and that matches a universal expectation that is independent of the injection and dissipation mechanisms as well as the boundary conditions strongly suggests that we have access here to intrinsic properties of the universal GP model Eq. (1).

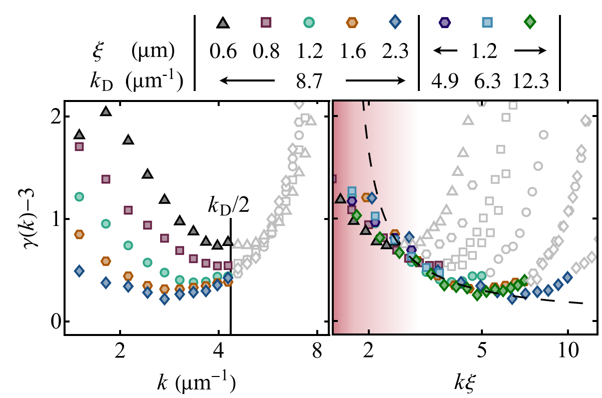

FIG. 5. The cascade exponent $\gamma(k)$ for different system parameters. (left) $\gamma(k)$ for different interactions is not universal, and it bends up around $k_D/2$ (solid line). (right) The rescaled data for γ versus $k\xi$ collapse in the range $2.5 \lesssim k\xi \lesssim k_D\xi/2$, demonstrating that the effective injection scale k_0 of the isotropic 4-wave cascade is $\propto k_\xi \equiv 1/\xi$. The dashed line shows the theoretical prediction $\gamma(k) - 3 = 1/[3\ln(k/k_0)]$ [20,33] with $k_0 = 1.64k_\xi$, and the red shading indicates the region of momentum space where the weak interaction approximation is not valid (see text).

Reconciling energy injection and dissipation rates—Here we study the ratio between energy injection rate ϵ_{in} and the *apparent* energy dissipation rate $\dot{N}U_D/V$ systematically by showing their ratio $\alpha = V\epsilon_{\mathrm{in}}/(\dot{N}U_D)$ for different U_s and a in Fig. 6. We find that the ratio is $\alpha \approx 1.3$, independent of U_s and has a weak dependence on a.

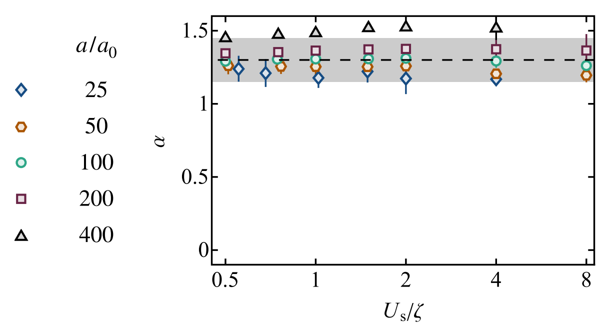

FIG. 6. The ratio α of ϵ_{in} and $\dot{N}U_D/V$ for different drive strengths U_s/ζ and scattering lengths a/a_0.

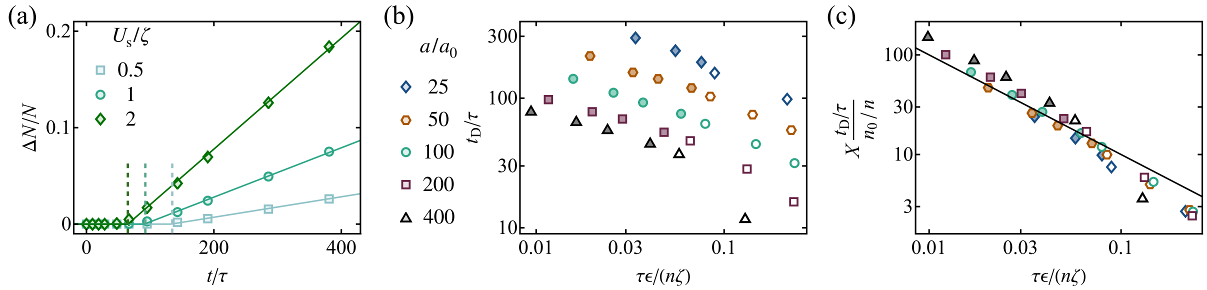

FIG. 7. The onset time for dissipation. (a) Number of particles lost from the system ΔN for different drive strengths U_s/ζ; here $a = 100a_0$. The lines are piece-wise linear fits, indicating that dissipation begins after a cascade build-up time t_D (vertical colored dashed lines). (b),(c) Onset time for dissipation t_D as a function of ϵ. (b) The relation is monotonic for a given interaction strength, but the data for t_D at different interaction strengths are not universal. (c) The onset times can be analytically calculated assuming that ϵ is constant over time [for the explicit expression of X, see Eq. (C1)]. The solid black line is the theoretical expectation $n\zeta/(\tau\epsilon)$. The closed (resp. open) symbols correspond to driving with $U_s \leq 1.5\zeta$ (resp. $U_s > 1.5\zeta$). For $U_s \leq 1.5\zeta$, the energy input rate is constant in time to within 10%.

The onset time for dissipation—Here we calculate the time t_D when the system starts to dissipate energy. As shown in Fig. S1 [38], the cascade front is not very sharp, so the onset of dissipation is not very sharp either [see Fig. 2(a)]. However, looking at the fractional particle loss $\Delta N/N$ instead, the onset is more clearly identifiable; to define t_D, we fit $\Delta N/N$ with a piecewise linear function and identify t_D as the singular point of the piecewise function [solid lines in Fig. 7(a)]. In Fig. 7(b), we show t_D versus ϵ for different a; t_D monotonically decreases with ϵ for a given interaction strength but the relation is not single valued for different a.

Remarkably, t_D can be calculated analytically under the assumption that the energy input rate is constant and that the onset of dissipation is sharp at $k = k_D$. As the momentum distribution has the form $n(k) = V/(2\pi)^3 n_0 k^{-3}(k\xi)^{-\gamma_0+3}$, the total energy of the system in the steady state is

$$\int_0^{k_D} 4\pi k^2 n(k) \frac{\hbar^2 k^2}{2m} \mathrm{d}k = n_0 \frac{U_D V (k_D \xi)^{3-\gamma_0}}{2\pi^2(5-\gamma_0)}.$$

Equating this to the energy injected into the system up until t_D yields

$$\frac{t_D}{\tau} = \frac{U_D (k_D\xi)^{3-\gamma_0}}{2\pi^2(5-\gamma_0)\zeta} \frac{n_0/n}{\tau\epsilon/n\zeta} \equiv X \frac{n_0/n}{\tau\epsilon/n\zeta}. \qquad \text{(C1)}$$

In Fig. 7(c) we show that t_D is in excellent agreement with this calculation for weak drives ($U_s \leq 1.5\zeta$), while for stronger drives the constant-ϵ assumption fails and t_D is shorter [open symbols in Fig. 7(c)]. Note that $t_D \propto U_D k_D^{3-\gamma_0} \propto k_D^{5-\gamma_0}$, is positive for our $\gamma_0 = 3.5$, meaning that $t_D \to \infty$ as $k_D \to \infty$. In the WWT language, this is referred to as an infinite capacity cascade [33]. This behavior is in stark contrast with the case of the K41 spectrum, where t_D is finite as $k_D \to \infty$ (more specifically, $t_D \sim t_D^{(0)} - A k_D^{-2/3}$ where A is a dimensionful constant).

Despite the weak nonlocality discussed in section "Sharpness of the cascade front," the dissipation onset time t_D matches the analytical prediction. In Fig. 2(a), we see that the curves for $\dot{N}U_D/N$ are slightly rounded before reaching their steady-state value but t_D is an approximate point of symmetry where the (unaccounted) energy dissipation before t_D matches the not yet fully saturated dissipation after t_D.